Albedos and diameters of three Mars Trojan asteroids

David E. Trilling [a], Andrew S. Rivkin [b], John A. Stansberry [a], Timothy B. Spahr [c], Richard A. Crudo [a,d], and John K. Davies [e]

[a] *Steward Observatory, The University of Arizona, 933 N. Cherry Avenue, Tucson, AZ 85721*

[b] *Applied Physics Laboratory, Johns Hopkins University, 11100 Johns Hopkins Road, Laurel, MD 20723*

[c] *Harvard-Smithsonian Center for Astrophysics, 60 Garden Street, Cambridge, MA 02139*

[d] *Present address: Department of Physics, University of Connecticut, U-3046, 2152 Hillside Road, Storrs, CT 06269*

[e] *UK Astronomy Technology Centre, Blackford Hill, Edinburgh, EH9 3HJ, UK*

Number of pages: 16

Number of tables: 2

Number of figures: 1

Preprint submitted to Icarus *25 June 2007*

Proposed Running Head:

Albedos and diameters of three Mars Trojans

Please send Editorial Correspondence to:

David E. Trilling

Steward Observatory

The University of Arizona

933 N. Cherry Avenue

Tucson, AZ 85721

Email: trilling@as.arizona.edu

Phone: (520) 626-1600

Fax: (520) 621-9555

ABSTRACT

We observed the Mars Trojan asteroids (5261) Eureka and (101429) 1998 VF_{31} and the candidate Mars Trojan 2001 FR_{127} at 11.2 and 18.1 microns using Michelle on the Gemini North telescope. We derive diameters of 1.36, 0.88, and $<$0.64 km, respectively, with corresponding geometric visible albedos of 0.35, 0.25, and $>$0.12. The albedos for Eureka and 1998 VF_{31} are consistent with the taxonomic classes and compositions (S(I)/angritic and S(VII)/achrondritic, respectively) and implied histories presented in a companion paper by Rivkin et al. Eureka's surface likely has a relatively high thermal inertia, implying a thin regolith that is consistent with predictions and the small size that we derive.

Keywords: TROJAN ASTEROIDS; INFRARED OBSERVATIONS; REGOLITHS

1 Introduction

It has been known for nearly a century that a large population of asteroids, known as Trojan asteroids, exists in a 1:1 resonance with Jupiter. Neptune is known to have five Trojan asteroids, but the only rocky planet with known Trojan asteroids is Mars. At present, the number of confirmed Mars Trojan asteroids is four, with a handful of other candidates. All but one orbit in the L5 (trailing) zone, with 1 in the L4 (leading) zone.

Mars Trojans can be dynamically stable over the age of the Solar System at inclinations between 12 and 40 degrees (Tabachnik and Evans, 1999; Scholl *et al.*, 2005); all known and candidate Mars Trojans reside in this dynamically stable region of phase space and may therefore be primordial objects. If so, these bodies represent leftover planetesimals from the formation of Mars. It is therefore interesting that there is evidence that suggests a diverse history for these bodies. Rivkin *et al.* (2003) obtained visible spectra of the three largest Mars Trojans — (5261) Eureka, (101429) 1998 VF_{31}, and (121514) 1999 UJ_7 — and found that Eureka and 1998 VF_{31} are likely Sa- or A-class asteroids, whereas 1999 UJ_7 is probably an X-class asteroid. These differing compositions suggest that these asteroids cannot have all formed in the same protostellar disk environment. Rivkin *et al.* (2007), a companion paper, extend the previous paper, finding that Eureka is angritic (igneous, from an oxidized, carbonaceous chondritic precursor), whereas 1998 VF_{31} is likely a primitive achondrite (from a reduced origin). The Rivkin spectra represent the total published knowledge of the physical properties of Mars Trojans. Clearly, additional data are needed to characterize these unique objects and unravel the population's history, since Mars Trojans may represent the only known planetesimals that formed interior

to the asteroid belt, and are the closest approximations to Earth's building blocks currently known.

We have obtained the first thermal infrared measurements of three Mars Trojan asteroids: (5261) Eureka, (101429) 1998 VF_{31}, and 2001 FR_{127} (this last being unconfirmed as a Mars Trojan due to lack of long-term dynamical integrations). Here we present our data (including some ancillary visible wavelength data); thermal modeling; and the resulting derived diameters and albedos. We briefly discuss the implications of our results, including their general agreement with the taxa presented in Rivkin *et al.* (2007).

2 Recovery of 2001 FR_{127}

2001 FR_{127} was discovered in March, 2001, and recovered two weeks later (Tichy *et al.*, 2001). On the basis of this arc, it was identified as a candidate Mars Trojan asteroid. (For simplicity, we refer this body hereafter simply as a Mars Trojan.) However, at the time of our Gemini observations four years later, the positional uncertainty for this object was around 0.67 degrees, far too large to be usefully targeted with Gemini/Michelle (see below), whose field of view is less than 1 arcminute. Before our thermal infrared observations could be carried out, therefore, 2001 FR_{127} needed to be recovered to reduce its positional uncertainty.

We carried out a wide-area recovery program in May and June, 2005, using `90prime`, the prime focus camera on the University of Arizona/Steward Observatory 90-inch (2.3-meter) Bok Telescope on Kitt Peak. `90prime` has an array of four 4096×4096 CCDs; the sides of the array span 1.16 deg, and the total

imaged area of the sky is 1 deg^2 per pointing (Williams *et al.*, 2004). We imaged a series of overlapping fields along the projected location of 2001 FR_{127}. We used a modified version of the Deep Ecliptic Survey data reduction and moving object detection pipeline (Millis *et al.*, 2002; Elliot *et al.*, 2005) to search for 2001 FR_{127}, and found it on multiple images. These new astrometric positions (Hergenrother *et al.*, 2005) allowed a substantial refinement of the orbital elements and a consequent reduction in positional uncertainty for 2001 FR_{127}. At the time of our Gemini observations of 2001 FR_{127} one month after recovery, the positional uncertainty was less than an arcsecond.

3 Partial lightcurve photometry

In order to detect or place limits on any visible lightcurves, we observed Eureka and 1998 VF_{31} in V band (predicted magnitudes from Horizons: 18.9 and 20.6, respectively) on 2005 Sep 19 UT with the facility 2K CCD (CCD21) imager on the Steward Observatory Mt. Bigelow 61-inch (1.54-meter) Kuiper Telescope. The night was not photometric, so we cannot independently determine the V magnitude of the asteroids. Each asteroid was easily detected in a series of 60 second exposures. 2001 FR_{127} was also attempted, but was too faint (predicted magnitude V=22.3 from Horizons) to be detected in 90 second exposures. Our time baseline was quite short – around 20 minutes for each of the two detected asteroids. No significant variation in flux from either asteroid was detected (using relative photometry to three comparably bright comparison stars that are nearby in the images). For the bright Eureka, our non-detection of flux variation places a 3σ limit on any lightcurve variation of 0.1 mag over the 20 minute observation window. This upper limit is consis-

tent with the Rivkin *et al.* (2003) measurement (from a different epoch) of a lightcurve amplitude at least 0.15 mag over around 6 hours. For the relatively faint 1998 VF_{31}, the 3σ limit on any lightcurve variation is around 1 magnitude over the 20 minute observation window. Both of these non-detections are useful in eliminating the possibility of fast rotations and extreme shapes, which would be suggested by large flux variations over these short time windows.

4 Thermal infrared observations

Mars Trojan asteroids Eureka, 1998 VF_{31}, and 2001 FR_{127} were observed in queue mode on 2005 Jul 6 (UT) at the Gemini North telescope on Mauna Kea using Michelle, a mid-infrared imager and spectrometer (Glasse *et al.*, 1997). In imaging mode, Michelle has a field of view of $32'' \times 24''$, with pixels 0.1 arcsec on a side. We used the N' ($\lambda_c = 11.2$ microns, $\Delta\lambda = 2.4$ microns) and Q_a ($\lambda_c = 18.1$ microns, $\Delta\lambda = 1.9$ microns) filters (see Table 1 for the observing log). The telescope was tracked at asteroid (non-sidereal) rates.

We employed the standard chop-nod strategy in which the telescope secondary chops (several Hertz) and the telescope nods (few times a minute) between nearby (8 arcsec) pointings in order to subtract out the thermal background from the telescope and atmosphere. The data was processed using the `midir` package of the Gemini IRAF package [1] . The `mireduce` task conveniently performs all the standard tasks of reorganizing data structures and stacking the chop-nod images to produce final double-differenced images. In each image stack for this program only a single target appears, at very close to its pre-

[1] Available at `http://www.gemini.edu/sciops/data/dataSoftware.html`

dicted location, so there is no confusion as to whether the measured source is the targeted source. The exceptions are the N' image of 2001 FR_{127} and the Q_a image of 1998 VF_{31}, in which no sources are evident at all; we derive upper limits to the fluxes for these two observations, as described below. In all cases, the images in the "off" positions are unguided and somewhat smeared, so we measure photometry from only the "on" (guided) positions. Each "on" source has one half of the total integration time.

Three photometric calibrator stars (see Cohen *et al.* (1999) and the Gemini web pages[2]) were observed using the same observing mode (Tables 1 and 2). For each standard star, we measured the total flux using aperture photometry. The extinction we derived from these calibration measurements is consistent with zero.

The Eureka and 1998 VF_{31} N' observations each were made with 24 total nods. For the Eureka observations, the image quality clearly degrades after the first 12 nods, so only these good quality images were used. For these data, we use a small centroided photometric aperture of 0.5 arcsec that is well-matched to the size of the image. This small aperture reduces the sky background noise included in the photometric aperture, but requires an aperture correction. We derive an aperture correction of 1.62 by measuring fluxes from the standard stars with both large and small apertures. The final (aperture corrected) N' flux for Eureka is given in Table 2.

1998 VF_{31} is somewhat fainter than Eureka, and is not visible in data from a single nod position. We used all 24 nod positions for this target, double-difference combined into three intermediate images of eight consecutive nod

[2] `http://www.gemini.edu/sciops/instruments/mir/MIRStdFluxes.html`

positions each. This allows us to make three independent measurements of the asteroid's brightness. The final (aperture corrected) N' flux for 1998 VF_{31} is given in Table 2.

At Q_a, Eureka is not visible in the data from individual nods nor easily visible in partial sums of the data. Consequently, we combine all the data into a single final double-differenced image. We used a small aperture of 0.7 arcsec, with an aperture correction of 1.23 (derived from the standard stars). The final (aperture corrected) Q_a flux for Eureka is given in Table 2.

We did not detect 1998 VF_{31} at Q_a band and did not detect 2001 FR_{127} at N' band. (Because 2001 FR_{127} was not detected at N', no measurement of that asteroid at Q_a was attempted.) To determine upper limits on the fluxes for these non-detections, we implanted scaled copies of the N' 1998 VF_{31} point source in the 2001 FR_{127} N' image and scaled copies of the Q_a Eureka point source in the 1998 VF_{31} Q_a image. We measure the fluxes for the faintest implanted objects that are detected to set the upper limits for these two observations. These limits are roughly consistent with three times the sky noise (Table 2), as expected.

Eureka is the brightest asteroid source in our program, and we look to it to characterize the errors in our measurements. We have 12 independent measurements of Eureka at N'. The scatter in these flux measurements is comparable to the variation in the sky background (both around 12%). We therefore conclude that, for measurements where we have only few or one flux measurement and hence cannot characterize the scatter in the measurements, we can estimate the error in our measurement from the sky variability. We use this technique for both the 1998 VF_{31} N' and Eureka Q_a measurements.

We convert Michelle counts to flux density units (mJy) by using the photometric calibrator stars (Table 2). We combine the measurements from all the calibrator stars to define a single calibration factor for each bandpass because the matches in time and sky location between calibration stars and asteroids are not very good. At N', the calibration factor is uncertain at the 5% level, as estimated from the scatter among the calibration factors from the three standard star measurements; at Q_a, the uncertainty, derived the same way, is around 10%. We add these errors in quadrature with the errors in our measurements to derive the final errors reported in Table 2.

Our targets have temperatures around 250 K (as calculated in our thermal modeling, described below). Thus, color corrections can be important, as these asteroids are substantially colder than the calibrator stars ($\sim$4000 K). The isophotal wavelengths (wavelength at which the flux density from the object's spectrum equals the average flux density calculated by integrating over the filter profile) for Ceres (217 K) in Michelle N' and Q_a are 11.52 microns and 18.26 microns, respectively (K. Volk, priv. comm.). We adopt these Ceres isophotal wavelengths for our observed asteroids as our derived temperatures are quite close to the Ceres temperature used. We use these isophotal wavelengths in our thermal models described below, although these shifts from nominal wavelengths are relatively small and, compared to the errors in our measurements, unimportant.

5 Thermal modeling and model results

We interpret the observed thermal emission from our targets using the Standard Thermal Model (STM; *e.g.* Lebofsky and Spencer (1989)). The STM

assumes a non-rotating (or zero thermal-inertia) spherical asteroid: dayside temperatures are in equilibrium with sunlight, while the nightside temperature is zero. Lebofsky *et al.* (1986) found that the thermal emission from asteroids frequently has a higher color temperature than would nominally be predicted under the STM assumptions given above, and introduced an empirical parameter, η, that allowed them to simultaneously model the elevated color temperature of the thermal emission and the (known) size of their targets (Ceres and Pallas). The canonical value for this beaming parameter η is 0.756, but recent studies (*e.g.* Harris (1998), Delbó and Harris (2002), Fernández *et al.* (2003), Stansberry *et al.* (2007)) find that η can be significantly larger.

We rely on JPL's Horizons ephemeris service for distance, phase angle, and absolute visual magnitude (H_V) information (Table 1, Table 2). We relate diameter, albedo, and H_V through

$$D = \frac{1329}{\sqrt{p_V}} \times 10^{-H_V/5} \tag{1}$$

where p_V is the visible geometric albedo and D is the diameter in kilometers (Harris, 1998). We use a thermal phase coefficient 0.01 mag/deg. We assume standard scattering behavior for the surface in the visible, resulting in a phase integral $q = 0.39$.

Our data on Eureka allow us to determine the albedo p_V, diameter D, and beaming parameter η, because Eureka is strongly detected at both N' and Q_a (in combination with H_V, this gives three measurements and three unknowns). Models with $\eta \simeq 1.5$ give the best fit $N' - Q_a$ color (by inspection), and albedo and diameter are derived with this constraint. The resulting fit gives $p_V = 0.35 \pm 0.11$ and $D = 1.36 \pm 0.25$ km (Figure 1 and Table 2). The

errors here result both from the errors in our mid-infrared photometry and an uncertainty of 0.3 mag for H_V (Jurić et al., 2002; Romanishin & Tegler, 2005), combined in quadrature. This derived albedo is consistent with the asteroid's S(I) taxonomic class and interpreted angritic composition (Rivkin *et al.*, 2007).

In the STM, dayside temperature goes as $\eta^{-1/4}$, so $\eta < 1$ results in warmer emission, while $\eta > 1$ results in cooler emission. Relatively cooler dayside temperatures will be produced by a high thermal inertia surface since some of the thermal emission will occur on the nightside. Thus, values of $\eta > 1$ are (somewhat ambiguous) evidence that thermal inertia plays a significant role in moderating diurnal variations in surface temperatures. We conclude from our $\eta = 1.5$ best fit that Eureka's surface may have a relatively high thermal inertia, consistent with a relative dearth of regolith (as predicted for bodies of this size (Binzel *et al.*, 2004; Cheng, 2005)) and with the small size we derive (*e.g.,* Delbó *et al.* (2007)).

Drawing upon the success of the STM in fitting the Eureka data, we apply the STM with $\eta = 1.5$ to the data for 1998 VF_{31} and 2001 FR_{127}; the results are shown in Figure 1. This extrapolation of the STM to these other two bodies is warranted both because the sizes and temperatures of these three asteroids do not differ significantly, and because the available data for 1998 VF_{31} and 2001 FR_{127} are so sparse that they do not justify a different model. Because we have only a single mid-infrared data point for 1998 VF_{31}, we solve for the albedo and diameter (Table 2) simply by finding the STM solution that passes through the N' measurement. For 2001 FR_{127}, we solve for the maximum radius (and minimum albedo) by finding the STM solution that passes through the N' upper limit measurement.

5.1 Thermal inertia on Eureka

Rivkin *et al.* (2003) determined that Eureka's rotation period is at least 6 hours. With this information and the derived albedo, we can constrain Eureka's thermal inertia, as follows.

Spencer *et al.* (1989) defined the dimensionless thermal parameter Θ, which gives the ratio of the characteristic radiation timescale to the diurnal (rotation) timescale:

$$\Theta = \Gamma \left[\frac{\left(\omega R^3\right)^2}{\epsilon\sigma \left[\left(1-A\right) S_1\right]^3} \right]^{\frac{1}{4}} \tag{2}$$

where Γ is the thermal inertia of the asteroid (units of J/m^2/K/sec$^{1/2}$); ω is the rotational frequency ($\omega = 2 * \pi / P$, where P is the rotational period); R is the heliocentric distance to the asteroid, in AU (Table 1); ϵ is the emissivity (we use $\epsilon = 0.9$); σ is the Stefan-Boltzmann constant; A is the bolometric albedo, which is $p_V \times q = 0.137$; and S_1 is the solar constant at 1 AU (we use 1366 W/m^2). Θ is zero for the STM (radiation timescale infinitely short compared to rotation timescale) and is infinite for the opposite end-member case where the rotation timescale is infinitely short compared to radiation timescale (i.e., fast rotation or high thermal inertia).

The STM implies that the radiation timescale is short compared to the rotation timescale; consequently, here $\Theta < 1$ (possibly, $\Theta \ll 1$). We can therefore rewrite Equation 2 to find the thermal inertia:

$$\Gamma < 98 \sqrt{\frac{P_h}{6 \text{ hours}}} \tag{3}$$

where P_h is the rotation period in hours. Based on the partial lightcurve given

in Rivkin *et al.* (2003), P_h could plausibly be two or even four times the minimum period of 6 hours, giving $\Gamma < 140$–200 J/m^2/K/sec$^{1/2}$, in excellent agreement with values obtained by Delbó *et al.* (2007) for comparably sized bodies.

This limit assumes that we are viewing Eureka equatorially. If Eureka's spin vector points somewhat toward the Sun, substantially larger thermal inertia values could be consistent with the data. In all cases, these relatively large values for thermal inertia imply a thin regolith for Eureka, consistent with our $\eta = 1.5$ solution and as expected from predictions (Binzel *et al.*, 2004; Cheng, 2005).

6 Summary and discussion

We observed the Mars Trojan asteroids Eureka, 1998 VF$_{31}$, and 2001 FR$_{127}$ at N' (11.2 microns) and Q_a (18.1 microns). Using the Standard Thermal Model, we derive diameters (albedos) of 1.36 km (0.35), 0.88 km (0.25), and <0.64 km (>0.12), respectively. Eureka's thermal inertia is constrained to be somewhat high relative to other Solar System objects, potentially implying a thin regolith, as predicted for a body this size.

Rivkin *et al.* (2007) find that Eureka is angritic and that 1998 VF$_{31}$ appears to be an S(VII) (e.g., primitive achondrite) asteroid. In both cases, the albedos we derive are consistent with those taxa and implied compositions.

2001 FR$_{127}$ has a diameter (<640 m) comparable to very small near Earth objects (NEOs) that have been observed in the mid-infrared (*e.g.*, Delbó *et al.* (2003)) and in radar experiments (*e.g.*, Ostro *et al.* (2002)). These are

among the smallest objects studied in the Solar System. By this virtue, further physical studies (spin, shape, lightcurve, etc.) are interesting on their own. Additionally, comparing physical properties between the dynamically old Mars Trojan asteroids studied here and the comparably sized but dynamically young NEOs may be useful in understanding the evolution of these smallest asteroids.

Acknowledgements

We thank Marco Delbó and Josh Emery for thoughtful, thorough, and helpful reviews. We thank Ed Olszewski and Grant Williams for their assistance with making `90prime` observations. Marc Buie developed the IDL moving object pipeline that was used to detect and measure the position for 2001 FR_{127}. Larry Wasserman helped with the modification of this pipeline for other observational platforms and also provided useful input on positional errors for planning the 2001 FR_{127} recovery observations. We thank Chad Engelbracht for helpful discussions about color corrections and Kevin Volk (Gemini) for providing the color corrections (isophotal wavelengths) for Michelle. We thank Tom Geballe, Scott Fisher, and Chad Trujillo (Gemini) and Rachel Mason and Michael Merrill (NOAO) for help with planning and carrying out the Gemini observations. This work is based in part on observations obtained at the Gemini Observatory, which is operated by the Association of Universities for Research in Astronomy, Inc., under a cooperative agreement with the NSF on behalf of the Gemini partnership: the National Science Foundation (United States), the Particle Physics and Astronomy Research Council (United Kingdom), the National Research Council (Canada), CONICYT (Chile), the Australian Research Council (Australia), CNPq (Brazil) and CONICET (Ar-

gentina). The data presented here were obtained under Gemini program GN-2005A-Q-47. We used the JPL Solar System Dynamics group's Horizons tool to plan our observations and analyze our results. This manuscript was prepared using the Elsevier/Icarus LaTeX template created by Ross Beyer et al. Finally, we are grateful to the indigenous people of Hawai'i for allowing astronomers to use their sacred mountain.

References

Binzel, R.P., Rivkin, A.S., Stuart, J.S., Harris, A.W., Bus, S.J., Burbine, T.H., 2004. Observed spectral properties of near-Earth objects: results for population distribution, source regions, and space weathering processes. Icarus 170, 259-294.

Cheng, A.F., 2004. Collisional evolution of the asteroid belt. Icarus 169, 357-372.

Cohen, M., Walker, R.G., Carter, B., Hammersley, P., Kidger, M., Noguchi, K., 1999. Spectral irradiance calibration in the infrared. X. A self-consistent radiometric all-sky network of absolutely calibrated stellar spectra. Astron. J. 117, 1864-1889.

Delbó, M. and Harris, A.W., 2002. Physical properties of near-Earth asteroids from thermal infrared observations and thermal modeling. Met. Planet. Sci. 37, 1929-1936.

Delbó, M., Harris, A.W., Binzel, R.P., Pravec, P., Davies, J.K., 2003. Keck observations of near-Earth asteroids in the thermal infrared. Icarus 166, 116-130.

Delbó, M., dell'Oro, A., Harris, A.W., Mottola, S., Mueller, M., 2007. Thermal inertia of near-Earth asteroids and implications for the magnitude of the

Yarkovsky effect. Icarus, in press.

Elliot, J.L., 10 colleagues, 2005. The Deep Ecliptic Survey: A search for Kuiper Belt Objects and Centaurs. II. Dynamical classification, the Kuiper Belt plane, and the core population. Astron. J. 129, 1117-1162.

Fernández, Y.R., Sheppard, S.S., Jewitt, D.C., 2003. The albedo distribution of Jovian Trojan asteroids. Astron. J. 126, 1563-1574.

Glasse, A.C., Atad-Ettedgui, E.I., Harris, J.W., 1997. Michelle midinfrared spectromneter and imager. Proc. SPIE 2871, 1197-1203.

Harris, A.W., 1998. A thermal model for near-Earth asteroids. Icarus 131, 291-301.

Hergenrother, C.W., Trilling, D.E., Spahr, T.B., 2005. MPEC 2005-L35.

Jurić, M., 15 colleagues, 2002. Comparison of Positions and Magnitudes of Asteroids Observed in the Sloan Digital Sky Survey with Those Predicted for Known Asteroids. Astron. J. 124, 1776-1787.

Lebofsky, L.A. and Spencer, J.R., 1989. Radiometry and thermal modeling of asteroids. In: Binzel, R.P., Gehrels, T., Matthews, M.S. (Eds.), Asteroids II, Univ. of Arizona Press, Tucson, pp. 128-147.

Lebofsky, L.A., Sykes, M.V., Tedesco, E.F., Veeder, G.J., Matson, D.L., Brown, R.H., Gradie, J.C., Feierberg, M.A., Rudy, R.J., 1986. A refined 'standard' thermal model for asteroids based on observations of 1 Ceres and 2 Pallas. Icarus 68, 239-251.

Millis, R.L., Buie, M.W., Wasserman, L.H., Elliot, J.L., Kern, S.D., Wagner, R.M., 2002. The Deep Ecliptic Survey: A search for Kuiper Belt Objects and Centaurs. I. Description of methods and initial results. Astron. J. 123, 2083-2109.

Ostro, S.J., Hudson, R.S., Benner, L.A.M., Giorgini, J.D., Magri, C., Margot, J.-L., Nolan, M.C., 2002. Asteroid radar astronomy. In: Bottke Jr., W.F.,

Cellino, A., Paolicchi, P., Binzel, R.P. (Eds.), Asteroids III, Univ. of Arizona Press, 151-168.

Rivkin, A.S., Binzel, R.P., Howell, E.S., Bus, S.J., Grier, J.A., 2003. Spectroscopy and photometry of Mars Trojans. Icarus 165, 349-354.

Rivkin, A.S., Trilling, D.E., Thomas, C.A., DeMeo, F., Spahr, T.B., Binzel, R.P., 2007. Composition of the L5 Mars Trojans: Neighbors, not Siblings. Icarus, submitted

Romanishin, W., Tegler, S. C., 2005. Accurate absolute magnitudes for Kuiper belt objects and Centaurs. Icarus, 179, 523-526.

Scholl, H., Marzari, F., Tricarico, P., 2005. Dynamics of Mars Trojans. Astron. Astroph. 175, 397-408.

Spencer, J.R., Lebofsky, L.A., Sykes, M.V., 1989. Systematic biases in radiometric diameter determinations. Icarus 78, 337-354.

Stansberry, J., Grundy, W., Brown, M., Cruikshank, D., Spencer, J., Trilling, D., Margot, J.-L., 2007. Physical properties of Kuiper Belt Objects and Centaurs: Spitzer Space Telescope constraints. In: Barucci, A., Boehnhardt, H., Cruikshank, D., Morbidello, A. (Eds.), The Kuiper Belt, Univ. of Arizona Press, in press

Tabachnik, S., Evans, N.W., 1999. Cartography for Martian Trojans. Ap. J. Lett. 517, L63-L66.

Tichy, M., 16 colleagues, 2001. MPEC 2001-F58.

Williams, G.G., Olszewski, E., Lesser, M.P., Burge, J.H., 2004. 90prime: a prime focus imager for the Steward Observatory 90-in. telescope. Proc. SPIE 5492, 787-798.

Observing log

Target	Filter	Obs. time (UT)	Exp. time (sec)	Airmass	R (AU)	Δ (AU)	phase (deg)
Eureka	N'	9.1675000	60	1.33	1.49	0.67	34.4
Eureka	Q_a	9.5359725	150	1.44	1.49	0.67	34.4
1998 VF_{31}	N'	10.783750	120	1.38	1.54	0.81	37.2
1998 VF_{31}	Q_a	11.152500	150	1.50	1.54	0.81	37.2
2001 FR_{127}	N'	11.989445	120	1.21	1.69	0.93	31.4
HD 141992	N'	8.7205560	15	1.07	···	···	···
HD 141992	Q_a	8.8315280	45	1.07	···	···	···
HD 156283	N'	11.471250	15	1.31	···	···	···
HD 158899	N'	12.296390	15	1.46	···	···	···
HD 158899	Q_a	12.407080	45	1.48	···	···	···

Table 1

All observations were made on 2005 Jul 06 (UT), with the exact midtimes indicated. The target asteroids and calibrator stars are given in the top and bottom groups, respectively. The exposure times used to measure object flux are listed here. The total open-shutter times, including both "on" and "off" (unguided) images, were 240 and 300 sec for asteroids and 30 and 90 sec for calibration stars at N' and Q_a, respectively. However, for all targets, only the "on" (guided) images were used, and for Eureka, the second half of the data was poor and not used.

Photometry and modeling results

Target	H (mag)	V (mag)	N' (mJy)	Q_a (mJy)	Albedo	Diameter (km)
Eureka	16.1	17.51	21.7 (2.8)	30.8 (4.8)	0.35 (0.11)	1.36 (0.25)
1998 VF_{31}	17.4	19.38	5.1 (0.9)	<15.4	0.25 (0.09)	0.88 (0.20)
2001 FR_{127}	18.9	21.21	<1.53	$\cdots$	>0.12	<0.64

Table 2

H magnitudes; V magnitudes at time of Michelle observations, from Horizons; measured fluxes at the isophotal wavelengths of 11.52 microns and 18.26 microns for N' and Q_a, respectively; and derived physical properties (using the modified STM). The uncertainty in H (and therefore V) is taken to be 0.3 mag. 1σ errors for our derived albedos and diameters are given in parentheses. These errors properly are not symmetric, but we do not believe that the uncertainties in the data and the model justify more rigorous error statements; here we present the more conservative values. No observation was made of 2001 FR_{127} at Q_a. These STM model results use $\eta = 1.5$. We used the following N' fluxes for photometric calibration: HD 141992, 13.586 Jy; HD 156283, 35.096 Jy; HD 158899, 11.754 Jy. We used the following Q_a fluxes for photometric calibration: HD 141992, 5.362 Jy; HD 158899, 4.650 Jy. (Photometric calibration fluxes from Cohen *et al.* (1999) and Gemini web pages.)

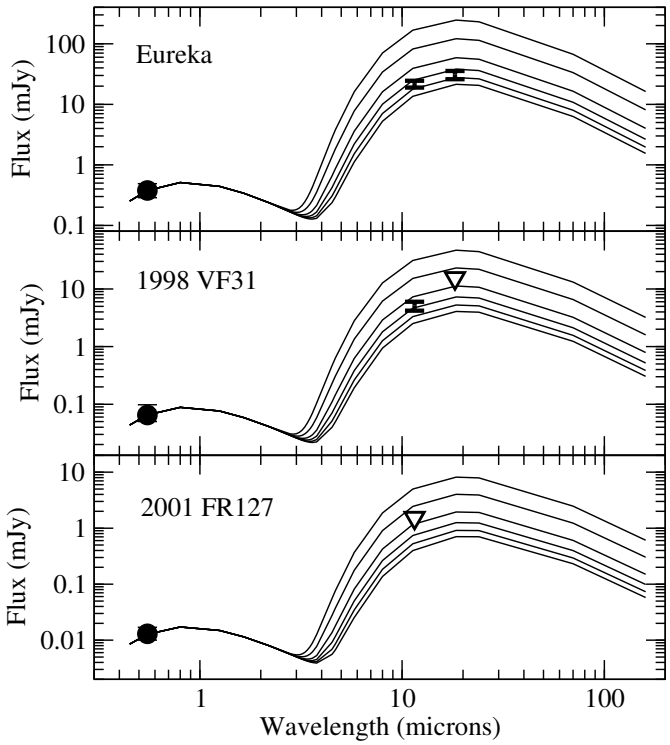

Fig. 1. Observed fluxes (plotted at isophotal wavelengths) and spectral energy distributions (solid curves) for the three observed Mars Trojans (as labeled), with STM solutions for a range of albedos and $\eta = 1.5$. Our detections are indicated by plotted error bars; upper limits are shown as downward pointing triangles. The isophotal wavelengths for these asteroids (temperatures around 250 K) are 11.52 and 18.26 microns for N' and Q_a, respectively (K. Volk, priv. comm.). Data in the visible (circles) is taken from JPL's Horizons service. (Error bars on the visible fluxes, corresponding to uncertainties in H of 0.3 magnitudes, are shown, but are generally smaller than the symbol size.) Based on our lack of detection of photometric variation (lightcurve), we assign no extra scatter to the reflected light (visible) data. For each case, we derive diameters from thermal fluxes (assuming $\eta = 1.5$ and derive albedo from the derived diameter and known H_V. Here we show models that correspond to six albedos: 0.05, 0.10, 0.20, 0.30, 0.40, and 0.50, from top to bottom, respectively. These models assume the nominal H values for each asteroid; larger H values imply smaller albedos and smaller H values give larger albedos.